Controlling Blend Film Morphology by Varying Alkyl Side Chain in Highly Coplanar Donor–Acceptor Copolymers for Photovoltaic Application

ARTICLE *in* MACROMOLECULES · AUGUST 2011

Impact Factor: 5.8 · DOI: 10.1021/ma201009n

Macromolecules

ARTICLE

pubs.acs.org/Macromolecules

Controlling Blend Film Morphology by Varying Alkyl Side Chain in Highly Coplanar Donor−Acceptor Copolymers for Photovoltaic Application

Yaowen Li, Yujin Chen, Xing Liu, Zhong Wang, Xiaoming Yang, Yingfeng Tu,* and Xiulin Zhu

Jiangsu Key Laboratory of Advanced Functional Polymer Design and Application, Department of Polymer Science and Engineering, College of Chemistry, Chemical Engineering and Materials Science, Soochow University, Suzhou, 215123, P. R. China

Supporting Information

ABSTRACT: A series of varied length alkyl substituted donor−acceptor (D−A) conjugated copolymers with benzo[1,2-*b*:4,5-*b*′]dithiophene (BDT) as donor and thiophene rings attached to both sides of the benzothiadiazole (TBT) moieties as acceptors were designed and synthesized. The optical and electrochemical properties showed that the absorption spectrum, the band gaps, and the energy levels of the copolymers were not affected by the varied substituted alkyls, and all these copolymers showed low band gaps around 1.75 eV. In addition, the morphologies of the blend film between copolymers and PCBM can be fine-tuned by increasing the length of substituted alkyl of the copolymers, changing from pea-like aggregation to interpenetrating network to grain-like aggregation. Bulk heterojunction photovoltaic devices were fabricated by using the copolymers as donors and (6,6)-phenyl C_{61}-butyric acid methyl ester ($PC_{61}BM$) or (6,6)-phenyl C_{71}-butyric acid methyl ester ($PC_{71}BM$) as acceptors. The optimized photovoltaic performances showed the stable open-circuit voltage (V_{oc}) in the range of 0.68 to 0.74 eV, and dramatically increasing short circuit current density (J_{sc}) by optimizing the blending morphologies of copolymer and PCBM films. The optimized photovoltaic performance with a V_{oc} of 0.70 V, J_{sc} of 7.19 mA/cm^2, a fill factor (*FF*) of 0.52, and a power conversion efficiency (PCE) of 2.88%, was obtained by the copolymer PBDT-TBT-C8 (PBDT-TBT-C8:$PC_{61}BM$, 1:3 w/w, in CB solution). This is due to its low band gap and interpenetrating network morphology of PBDT-TBT-C8:$PC_{61}BM$ blend film. The photovoltaic device based on PBDT-TBT-C8:$PC_{71}BM$ showed a J_{sc} of 8.6 mA/cm^2 and a PCE of 3.15%.

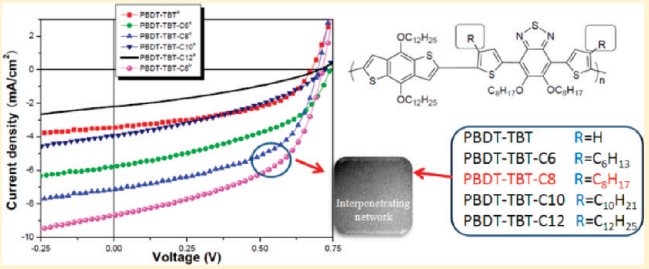

INTRODUCTION

In recent years, considerable efforts have been directed toward the development of new photovoltaic polymers, which are becoming more and more attractive because they represent low cost and flexible devices, tunable electronic properties, and ease of processing.[1−3] At present, polymer photovoltaic cells (PVCs) with a bulk heterojunction (BHJ) active layer have been proven to be the most successful. The fundamental concept of BHJ polymer PVCs involves the self-assembly of nanoscale heterojunctions by spontaneous phase separation of the donor (polymer) and the acceptor (fullerene), resulting in the formation of heterojunctions, or an interpenetrating network throughout the bulk of the donor and acceptor molecules.[4] Over the past decade, much progress has been made for BHJ PVCs based on regioregular poly(3-hexylthiophene) (P3HT) and PCBM.[5−7] However, the relatively large band gap of P3HT (∼1.9 eV) limits the fraction of the solar spectrum that can be harvested, as well the relatively small energy difference between the highest occupied molecular orbital (HOMO) of P3HT and the lowest unoccupied molecular orbital (LUMO) of the fullerene acceptor results in a low open-circuit voltage (0.6 V). In order to get improved performance of PVCs, the donor and acceptor molecules in the active layer must possess better intrinsic absorption properties, desirable HOMO/LUMO energy levels, and higher photocurrent generation. To conquer these problems, low-bandgap (LBG) polymers have been utilized recently in PVCs with fullerene derivatives, such as $PC_{61}BM$ or $PC_{71}BM$, yielding better PCE values up to 7.7%.[8−11] It is notable that most of the promising electron donor materials are composed of electron-donating (donor) and electron-accepting (acceptor) units, which possess low band gaps and deeper HOMO energy levels.[12−14] Meanwhile, incorporation of wide ranges of donors and acceptors into LBG polymers can manipulate the electronic structures. The interaction between electron-donating moiety and electron-accepting moiety forms the intramolecular charge transfer (ICT) transition leading to newly formed high-lying HOMO and low-lying LUMO, which can also account for the reduced optical absorption band gap.[15,16]

BHJ solar cells based on semiconducting polymers are complex systems. Their performances are not only affected by the

Received: May 3, 2011
Revised: July 22, 2011
Published: August 02, 2011

electrical properties of donor polymers, but also by many other factors, e.g., interaction of donor polymers and acceptors, morphology of the blend films, interfacial properties, and electrodes.[17−19] All these factors are crucial for the charge transfer and collection. By blending donor and acceptor materials together, an interpenetrating network with a large D−A interfacial area, which is regarded as ideal morphology for BHJ solar cells, can be achieved through controlling the phase separation between the two components in bulk. In this way, any absorbing site in the composite is within 10−15 nm of the donor−acceptor phase separation, and the formation of a bicontinuous network creates two channels to transport holes in the donor domain and electrons in the acceptor domain, leading to much enhanced quantum efficiency of charge separation.[20] In addition, the strong driving force for the development of long-range order aided by the coplanarity of the polymer backbone, which generally exhibit better $\pi-\pi$ stacking and higher carrier mobility in solid state, favors the exclusion of the fullerene and induces a large extent of phase segregation in a blend film with the fullerene. Therefore, among these factors, the morphology control of the blend film plays an important role. To achieve high solar power conversion efficiency (PCE), several effective methods have been developed to optimize the phase separation formed by the electron donor and acceptor molecules, including thermal annealing,[21] and solvent mixtures[22] or additives.[23] However, these methods are not all-purpose because of their complicated mechanism in tuning the morphology. Generally, all the above methods are adopted to tune the morphology one after the other, which greatly increases the cost and periods of the devices fabrication.

In view of the disadvantage of postprocessing method for the morphology control of the active layer, polymer chemical modification affords various useful strategies for changing its solubility, coplanarity of the conjugated main chain and the miscibility between the donor polymer and fullerene derivative acceptor, which can adjust intermolecular interactions and self-assembly ability of the composite to form the desirable morphology. To our knowledge, there have been several reports on the morphology control of the blend film by modification polymer donor and the photovoltaic performance has been greatly improved. Most recently, Yu et al.[9] reported incorporating fluorine into the various positions of the polymer backbone can significantly affect the morphology of the polymer/$PC_{71}BM$ blend film by changing from spherical domain to uniform and fine features, and the solar cells' power conversion efficiency were improved from 2.3% to 7.2%. Meanwhile, our recent work has succeeded in developing a series of low band gap D−A copolymers with varied ratios of two different electron-accepting moieties, which exhibit different self-assembly characteristics when blend with PCBM. The morphologies of the blend film were also tuned from a grain-like aggregation to an interpenetrating network to a club-like structure, and the corresponding devices showed an improvement PCEs from 0.68 to 2.89%.[24] In addition, there are several reports about the effect of varied donor copolymer side chains on the blend film (polymer and PCBM) morphology, where it can significantly impact structural order, orientation in polymer backbones and $\pi-\pi$ stacking interactions in the polymer domains, and critically affecting device performance.[25−27] On all accounts, the blend film morphology between donor and acceptor plays an important role in the performance of PVCs.

In order to further develop the chemical modification method for controlling the blend film morphology, enhancing the $\pi-\pi$ stacking interactions between polymer and PCBM, and hence obtain potential photovoltaic materials, we construct a series high coplanarity D−A based low band gap copolymers. The benzo[1,2-*b*:4,5-*b*′]dithiophene (BDT) and benzothiadiazole (BT) are generally considered highly coplanar electron-donating and electron-accepting moieties, respectively. As a result of less steric hindrance and easily formed $\pi-\pi$ stacking, the incorporation of BDT and BT moiety not only induces more intense electronic transitions in the entire visible range to broaden the absorption bandwidth and reduce the band gap, but also improves the hole mobility.[28,29] In addition, the BDT and BT moieties were bridged by a conjugated moiety, which can be expected to enhance the conjugated length, broaden the absorption spectrum, and improve the hole mobility of the copolymers. Because of the bad solubility of copolymers with rigid backbone, flexible alkoxyl or alkyl chains was introduced on the copolymers to improve the solubility. Meanwhile, considering the fact that varied types and attached position of flexible chain may cause the different solubility of copolymers, the miscibility between copolymer and PCBM, and the twist of the backbone, a better selection of the attached flexible chain on the backbone of the copolymers may realize the control of the blend film morphology between copolymer and PCBM.

On the basis of the above idea, a series of high coplanar D−A copolymers consisting of alkoxy substituted BDT (alkoxy-BDT) with no substituent on 1, 3, 5, and 7 positions were designed as the donor, which makes BDT an ideal conjugated unit for new photovoltaic materials. The alkoxy substituted 2,1,3-benzothiadiazoles were chosen as electron-accepting moiety, and it connected with thiophene units to give compounds (TBT) from M-1 to M-5 copolymerizing with alkoxy-BDT. In order to fine-tune the $\pi-\pi$ stacking effect and self-assembly ability properties, five copolymers with varied alkyl length attaching to thiophene moiety were designed and synthesized. Both the UV−visible absorption spectra and electrochemical properties of the copolymers exhibited low band gaps around 1.75 eV. Meanwhile, the substituted varied alkyl length on the thiophene moiety can not only keep their low band gap but also give a stable HOMO and LUMO energy level. Furthermore, with the increasing substituted alkyl length, the morphology of the blend films between copolymers and $PC_{61}BM$ exhibited different self-assembly characteristics, changing from pea-like aggregation to interpenetrating network to grain-like aggregation. The optimized photovoltaic performance under AM1.5 conditions with a V_{oc} of 0.70 V, J_{sc} of 7.19 mA/cm^2, a fill factor (FF) of 0.52, and a power conversion efficiency (PCE) of 2.88%, was obtained by the copolymer PBDT-TBT-C8 (PBDT-TBT-C8:$PC_{61}BM$, 1:3 w/w, in CB-solution) due to its interpenetrating network morphology of PBDT-TBT-C8:$PC_{61}BM$ blend film. Additionally, the photovoltaic device based on PBDT-TBT-C8:$PC_{71}BM$ showed a J_{sc} of 8.6 mA/cm^2 and PCE of 3.15%.

EXPERIMENTAL SECTION

Materials and Synthesis. 2,6-Bis(trimethyltin)-4,8-didodecyloxybenzo[1,2-*b*;3,4-*b*]dithiophene was synthesized according to Hou et al. reported.[30] All reagents and chemicals were purchased from commercial sources (Aldrich, Across, Fluka) and used without further purification unless stated otherwise. All solvents were distilled over appropriate drying agent(s) prior to use and were purged with nitrogen.

1,2-Bis(octyloxy)benzene (1). To a solution of catechol (5.0 g, 45.0 mmol) in dry DMF (40 mL) were added 1-bromooctane (20.3 g, 18.2 mL, 105 mmol,) and K_2CO_3 (19 g, 135 mmol). The mixture was stirred at 100 °C under a nitrogen atmosphere for 48 h. After cooling the

mixture to room temperature (RT), 80 mL of water were added. The aqueous layer was extracted with CH_2Cl_2 and the organic layer was separated. The organic extracts were dried over anhydrous $MgSO_4$, evaporated and purified with column chromatography on silica gel with CH_2Cl_2: petroleumether (1:10) as the eluent to give white solid 12.8 g (38.3 mmol, yield 85%). ^{1}H NMR (500 MHz, $CDCl_3$, TMS): δ (ppm) 6.86 (s, 4H, −Ph), 3.98 (t, 4H, J = 6.75 Hz, $-OCHH_2$), 1.81 (m, 4H, $-CH_2$), 1.47 (m, 4H, $-CH_2$), 1.34 (m, 16H, $-CH_2$), 0.89 (t, 16H, J = 6.75, $-CH_3$). Anal. Calcd for $C_{22}H_{38}O_2$: C, 78.99; H, 11.45. Found: C, 78.95; H, 11.47.

1,2-Dinitro-4,5-bis(octyloxy)benzene (2). To a two neck round-bottom flask containing dichloromethane (140 mL), acetic acid (140 mL), and 1,2-bis(octyloxy)benzene (6.7 g, 19.9 mmol) cooled to 10 °C was added dropwise 65% nitric acid (20 mL). The reaction was allowed to warm to room temperature and stirred for 1 h. The mixture was again cooled to 10 °C and 100% nitric acid (50 mL) was added dropwise. The mixture was allowed to warm to room temperature and the mixture was stirred for 40 h. After completion of the reaction, the reaction mixture was poured into ice−water and the dichloromethane layer was separated. The water phase was extracted with dichloromethane. The combined organic phase was washed with water, saturated $NaHCO_3$ (aq), and brine and dried over $MgSO_4$. Concentration in vacuum gave the crude product and was recrystallized from ethanol, obtained yellow solid 7.8 g (18.3 mmol, yield 92%). ^{1}H NMR ($CDCl_3$, 300 MHz): δ (ppm) 7.30 (s, 2H, −Ph), 4.10 (t, J = 8.8 Hz, 4H, $-OCHH_2$), 1.88 (m, 4H, $-CH_2$), 1.48 (m, 4H, $-CH_2$) 1.294 (m, 16H, $-CH_2$), 0.88 (t, J = 6.6 Hz, 6H, $-CH_3$). Anal. Calcd for $C_{22}H_{38}O_2$: C, 62.24; H, 8.55. Found: C, 62.21; H, 8.60.

5,6-Bis(octyloxy)benzo[*c*][1,2,5]thiadiazole (3). A mixture of 1,2-dinitro-4,5-bis(octyloxy)benzene (1.43 g, 3.37 mmol) and $Sn^{II}Cl_2 \cdot 2H_2O$ (6.07 g, 26.9 mmol) in ethanol (50 mL) and concentrated HCl (20 mL) was heated to 85 °C overnight. After cooling to room temperature, the product was filtered and washed with water and methanol. Finally it was dried at RT under a stream of argon and used directly. To a mixture of 4,5-bis(octyloxy)benzene-1,2-diaminium chloride (1.11 g, 2.54 mmol) and triethylamine (25.1 mmol, 3.5 mL) in 40 mL of dichloromethane was slowly added a solution of thionyl chloride (4.83 mmol, 352 μL) in 5 mL of dichloromethane. After addition, the mixture was heated to reflux for 6 h. The cooled solution was concentrated in vacuum followed by trituration in water. After the solution was stirred for 30 min, the product was filtered off and recrystallized from ethanol and gave off-white solid 0.63 g (yield 62%). ^{1}H NMR ($CDCl_3$, 300 MHz): δ (ppm) 7.14 (s, 2H, -Ph), 4.09 (t, J = 6.6 Hz, 4H, $-OCHH_2$), 1.92 (m, 4H, $-CH_2$), 1.52 (m, 4H, $-CH_2$), 1.30 (m, 16H, $-CH_2$), 0.89 (t, J = 9.0 Hz, $-CH_3$) ^{13}C NMR ($CDCl_3$, 75 MHz): δ (ppm) 154.1, 151.3, 98.4, 69.1, 31.8, 29.3, 29.2, 28.7, 25.1, 22.6, 14.1.

4,7-Dibromo-5,6-bis(octyloxy)benzo[*c*][1,2,5]thiadiazole (4). To a solution of **3** (4.6 g, 11.7 mmol) in a mixture of dichloromethane (328 mL) and acetic acid (144 mL) was added bromine (4.1 mL, 80 mmol), and the resulting mixture was stirred in the dark for ca. 48 h at room temperature. The mixture was then poured into water (400 mL), extracted with dichloromethane, sequentially washed with water, saturated $NaHCO_3$ (aq), and 1 M Na_2SO_3 (aq), and the solvents were evaporated off under reduced pressure. The crude product was purified by recrystallization from ethanol twice to give needle-like crystals 4.76 g (yield 74%). ^{1}H NMR ($CDCl_3$, 300 MHz): δ (ppm) 4.16 (t, J = 6.75 Hz, 4H, $-OCHH_2$), 1.89 (m, 4H, $-CH_2$), 1.56 (m, 4H, $-CH_2$), 1.36 (m, 16H, $-CH_2$), 0.91 (t, J = 6.9 Hz, 6H, $-CH_3$). ^{13}C NMR ($CDCl_3$, 75 MHz): δ (ppm) 154.2, 150.1, 106.0, 74.9, 31.6, 30.1, 29.2, 29.1, 25.8, 22.5, 13.9.

5,6-Bis(octyloxy)-4,7-di(thiophen-2-yl)benzo[*c*][1,2,5]-thiadiazole (M-1). To a solution of **4** (0.6 g, 1.09 mmol), Pd-$(PPh_3)Cl_2$ (38 mg, 0.05 mmol) in dry THF (20 mL) was added 2-tributylstannylthiophene (1.23 g, 3.3 mmol) and the reaction mixture was heated to reflux for 24 h under argon. The reaction mixture was concentrated, then purified with column chromatography on silica gel with CH_2Cl_2: petroleumether (1:3) as the eluent to give orange solid 473 mg (78%). ^{1}H NMR ($CDCl_3$, 400 MHz): δ (ppm) 8.48 (d, J = 3.6 Hz, 2H, −Th), 7.51 (d, J = 4.8 Hz, 2H, −Th), 7.24 (m, 2H, −Th), 4.12 (t, J = 7.1 Hz, 4H, $-OCHH_2$), 1.93 (m, 4H, $-CH_2$), 1.45 (m, 4H, $-CH_2$), 1.33 (br, 16H, $-CH_2$), 0.91 (m, 6H, $-CH_2$). ^{13}C NMR ($CDCl_3$, 100 MHz): δ (ppm) 152.0, 151.1, 134.2, 130.7, 127.4, 126.8, 117.7, 74.4, 32.0, 30.5, 29.7, 29.4, 26.1, 22.8, 14.3.

4,7-Bis(4-hexylthiophen-2-yl)-5,6-bis(octyloxy)benzo[*c*]-[1,2,5]thiadiazole (M-2). This compound was prepared with the same procedure according to **M-1**. ^{1}H NMR ($CDCl_3$, 400 MHz): δ (ppm) 8.31 (s, 2H, −Th), 7.09 (s, 2H, -Th), 4.10 (t, J = 7.0 Hz, 4H, $-OCHH_2$), 2.72 (t, J = 7.6 Hz, 4H, $-CH_2$), 1.92 (m, 4H, $-CH_2$), 1.72 (m, 4H, $-CH_2$), 1.43 (m, 8 H, $-CH_2$), 1.34 (br, 24 H, $-CH_2$), 0.91 (m, 12 H, $-CH_3$). ^{13}C NMR ($CDCl_3$, 100 MHz): δ (ppm) 152.1, 151.1, 143.0, 134.0, 132.1, 122.4, 117.7, 74.4, 32.0, 31.9, 30.8, 30.7, 30.6, 29.8, 29.5, 29.3, 26.2, 22.9, 22.8, 14.3.

5,6-Bis(octyloxy)-4,7-bis(4-octylthiophen-2-yl)benzo[*c*]-[1,2,5]thiadiazole (M-3). This compound was prepared with the same procedure according to **M-1**. ^{1}H NMR ($CDCl_3$, 400 MHz): δ(ppm) 8.31 (s, 2H, −Th), 7.10 (s, 2H, −Th), 4.10 (t, J = 7.0 Hz, 4H, $-OCHH_2$), 2.72 (t, J = 7.8 Hz, 4H, $-CH_2$), 1.93 (m, 4H, $-CH_2$), 1.72 (m, 4H, $-CH_2$), 1.65 (m, 4 H, $-CH_2$), 1.34 (br, 36 H, $-CH_2$), 0.90 (m, 12 H, $-CH_3$).

4,7-Bis(4-decylthiophen-2-yl)-5,6-bis(octyloxy)benzo[*c*]-[1,2,5]thiadiazole (M-4). This compound was prepared with the same procedure according to **M-1**. ^{1}H NMR ($CDCl_3$, 400 MHz): δ (ppm) 8.34 (s, 2H, −Th), 7.12 (s, 2H, -Th), 4.12 (t, J = 7.0 Hz, 4H, $-OCHH_2$), 2.73 (t, J = 7.6 Hz, 4H, $-CH_2$), 1.94 (m, 4H, $-CH_2$), 1.73 (m, 4H, $-CH_2$), 1.30 (m, 48 H, $-CH_2$), 0.92 (m, 12 H, $-CH_3$). ^{13}C NMR ($CDCl_3$, 100 MHz): δ (ppm) 152.0, 151.1, 143.0, 133.9, 132.1, 122.4, 117.7, 74.4, 32.1, 32.0, 30.8, 30.6, 29.8, 29.7, 29.6, 29.5, 29.5, 28.4, 26.9, 26.2, 22.9, 17.4, 14.3, 13.8.

4,7-Bis(4-dodecylthiophen-2-yl)-5,6-bis(octyloxy)benzo-[*c*][1,2,5]thiadiazole (M-5). This compound was prepared with the same procedure according to **M-1**. ^{1}H NMR ($CDCl_3$, 400 MHz): δ(ppm) 8.34 (s, 2H, −Th), 7.12 (s, 2H, −Th), 4.12 (t, J = 7.0 Hz, 4H, $-OCHH_2$), 2.73 (t, J = 7.8 Hz, 4H, $-CH_2$), 1.95 (m, 4H, $-CH_2$), 1.74 (m, 4H, $-CH_2$), 1.66 (m, 4H, $-CH_2$), 1.28 (m, 52 H, $-CH_2$), 0.92 (m, 12 H, $-CH_3$). ^{13}C NMR ($CDCl_3$, 100 MHz): δ (ppm) 152.0, 151.1, 143.0, 133.9, 132.1, 122.4, 117.7, 74.4, 32.1, 32.0, 30.8, 30.6, 29.9, 29.8, 29.7, 29.7, 29.6, 29.5, 29.5, 28.4, 26.9, 26.2, 22.9, 17.4, 14.3, 13.8.

4,7-Bis(5-bromothiophen-2-yl)-5,6-bis(tetradecyloxy)-benzo[*c*][1,2,5]thiadiazole (BM-1). To a solution of **5** (760 mg, 1.37 mmol) in $CHCl_3$ (48 mL) and glacial acetic acid (48 mL) was added NBS (2.73 mmol, 485 mg) in one portion. The mixture was stirred at room temperature for 20 h in the dark. The reaction mixture was concentrated directly on Celite in vacuum and then purified with column chromatography on silica gel with CH_2Cl_2:petroleum ether (1:3) as the eluent to give an orange solid in 832 mg (85%) yield. ^{1}H NMR ($CDCl_3$): δ = 8.41 (s, 2H, -Th), 7.22 (s, 2H, −Th), 4.12 (br, 4H, $-OCHH_2$), 2.00 (m, 4H, $-CH_2$), 1.51 (br, 20H, $-CH_2$), 0.96 (m, 6H, $-CH_2$). ^{13}C NMR ($CDCl_3$, 100 MHz): δ (ppm)151.6, 150.5, 135.8, 131.1, 129.8, 117.1, 115.6, 74.7, 32.0, 30.4, 29.6, 29.4, 26.1, 22.8, 14.3.

4,7-Bis(5-bromo-4-hexylthiophen-2-yl)-5,6-bis(octyloxy)-benzo[*c*][1,2,5]thiadiazole (BM-2). This compound was prepared with the same procedure according to **BM-1**. ^{1}H NMR ($CDCl_3$, 400 MHz): δ (ppm) 8.35 (s, 2H, -Th), 4.15 (t, J = 6.6 Hz, 4H, $-OCHH_2$), 2.70 (t, J = 7.4 Hz, 4H, $-CH_2$), 1.99 (m, 4H, $-CH_2$), 1.72 (m, 4H, $-CH_2$), 1.38 (br, 32H, $-CH_2$), 0.94 (m, 12 H, $-CH_3$). ^{13}C NMR ($CDCl_3$, 100 MHz): δ (ppm) 151.6, 150.5, 141.8, 133.9, 131.7, 117.0, 112.8, 74.5, 32.0, 31.9, 30.5, 30.0, 29.8, 29.7, 29.5, 29.2, 26.2, 22.9, 22.9, 14.3.

Scheme 1. Synthesis of Monomers and Copolymers

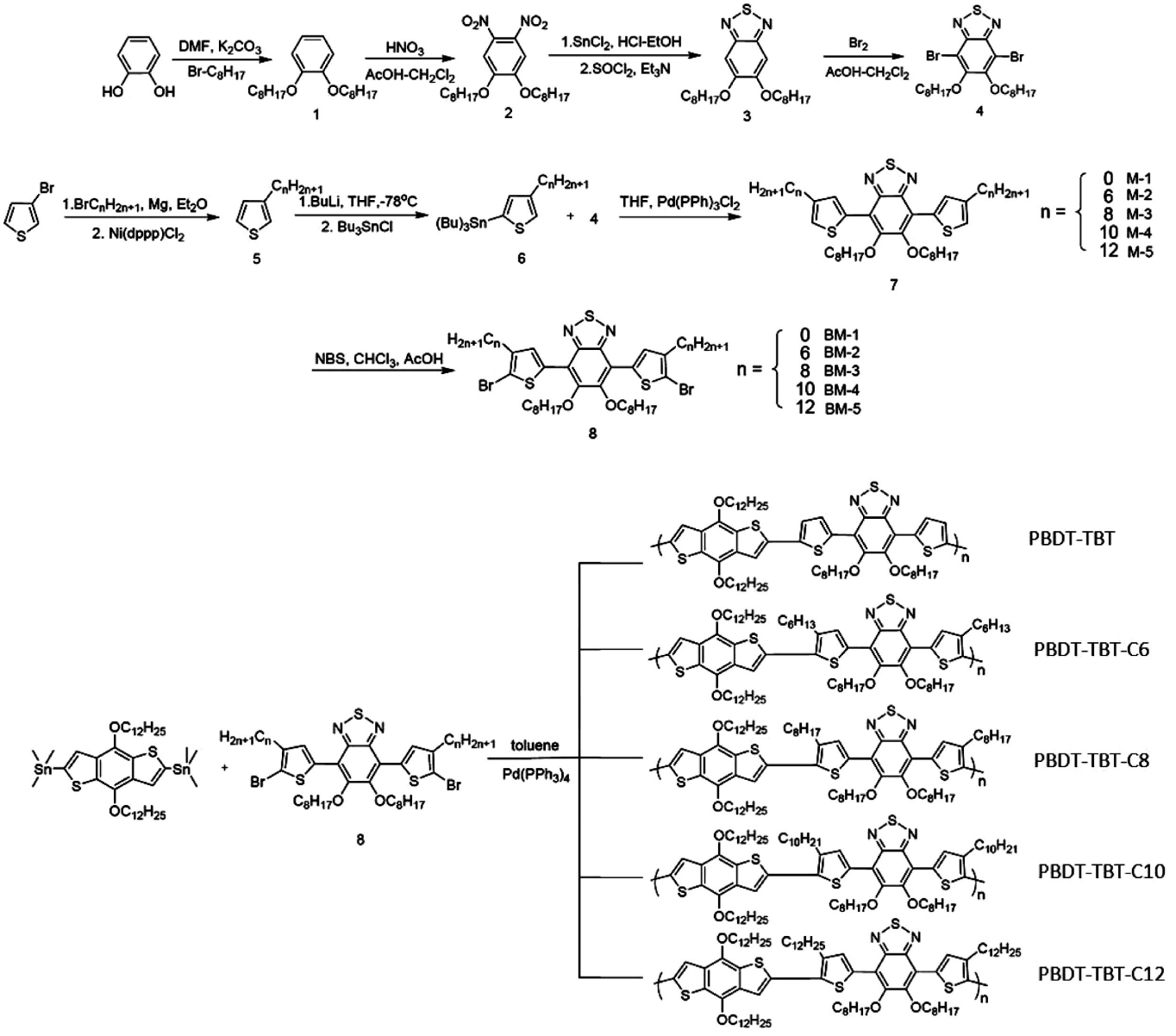

4,7-Bis(5-bromo-4-octylthiophen-2-yl)-5,6-bis(octyloxy)-benzo[*c*][1,2,5]thiadiazole (BM-3). This compound was prepared with the same procedure according to **BM-1**. ^{1}H NMR ($CDCl_3$, 400 MHz): δ (ppm) 8.32 (s, 2H, -Th), 4.13 (t, J = 6.2 Hz, 4H, $-OCHH_2$), 2.67 (t, J = 6.8 Hz, 4H, $-CH_2$), 1.96 (m, 4H, $-CH_2$), 1.70 (m, 4H, $-CH_2$), 1.31 (br, 40H, $-CH_2$), 0.91 (m, 12 H, $-CH_3$). ^{13}C NMR ($CDCl_3$, 100 MHz): δ (ppm) 151.6, 150.5, 141.8, 133.9, 131.7, 117.0, 112.8, 74.5, 32.1, 32.0, 30.5, 30.1, 29.8, 29.7, 29.6, 29.6, 29.5, 26.2, 22.9, 14.3.

4,7-Bis(5-bromo-4-decylthiophen-2-yl)-5,6-bis(octyloxy)-benzo[*c*][1,2,5]thiadiazole (BM-4). This compound was prepared with the same procedure according to **BM-1**. ^{1}H NMR ($CDCl_3$, 400 MHz): δ (ppm) 8.33 (s, 2H, -Th), 4.13 (t, J = 7 Hz, 4H, $-OCHH_2$), 2.67 (t, J = 7.6 Hz, 4H, $-CH_2$), 1.96 (m, 4H, $-CH_2$), 1.70 (m, 4H, $-CH_2$), 1.29 (br, 48H, $-CH_2$), 0.89 (m, 12 H, $-CH_3$). ^{13}C NMR ($CDCl_3$, 100 MHz): δ (ppm) 151.5, 150.4, 141.8, 133.9, 131.7, 116.9, 112.8, 74.5, 53.6, 32.1, 32.1, 30.6, 30.1, 29.9, 29.8, 29.8, 29.7, 29.6, 29.5, 26.2, 22.9, 14.3.

4,7-Bis(5-bromo-4-dodecylthiophen-2-yl)-5,6-bis(octyloxy)-benzo[*c*][1,2,5]thiadiazole (BM-5). This compound was prepared with the same procedure according to **BM-1**. ^{1}H NMR ($CDCl_3$, 400 MHz): δ (ppm) 8.33 (s, 2H, $-$Th), 4.13 (t, J = 7 Hz, 4H, $-OCHH_2$), 2.67 (t, J = 7.6 Hz, 4H, $-CH_2$), 1.96 (m, 4H, $-CH_2$), 1.69 (m, 4H, $-CH_2$), 1.27 (br, 56H, $-CH_2$), 0.89 (m, 12 H, $-CH_3$). ^{13}C NMR ($CDCl_3$, 100 MHz): δ (ppm) 151.6, 150.6, 141.9, 133.9, 131.7, 117.0, 112.7, 74.6, 32.1, 32.0, 30.5, 30.0, 29.9, 29.8, 29.7, 29.6, 29.5, 29.4, 29.1, 29.0, 28.4, 26.9, 26.1, 22.9, 14.1, 13.6.

General Procedures of Polymerization. Stille cross-coupling reaction was used to synthesize the copolymers as shown in Scheme 1. The 5,6-bis(octyloxy)-4,7-di(thiophen-2-yl)benzo[*c*][1,2,5]thiadiazole with different alkyl chains, 2,6-bis(trimethyltin)-4,8-didodecyloxybenzo-[1,2-b;3,4-b]dithiophene (BDT) and $(PPh_3)_4Pd(0)$ (2 mol % with respect to the monomer BM) as the catalyst precursor were dissolved in a mixture of toluene (15 mL). The solution was stirred under Ar atmosphere and refluxed with vigorous stirring for 24 h. The resulting solution was then poured into methanol and followed by washing with water. The

precipitated solid was extracted with methanol and acetone for 24 h in a Soxhlet apparatus to remove the oligomers and catalyst residues, respectively. The soluble fraction was then collected via extraction with chloroform for 24 h. The chloroform solution was then concentrated to afford the copolymers.

Poly{4,8-didodecyloxybenzo[1,2-*b*;3,4-*b*]dithiophene-*alt*-5,6-bis(octyloxy)-4,7-di(thiophen-2-yl)benzo[*c*][1,2,5]-thiadiazole} (PBDT-TBT). The resulting copolymer PBDT-TBT was obtained as a dark powder with a yield of 72%. ^{1}H NMR (400 MHz, $CDCl_3$): δ (ppm) 8.56 (br, 2H, −Th), 7.43 (br, 4H, −Th), 4.33 (br, 4H, $-OCHH_2$), 4.21 (br, 4H, $-OCHH_2$), 1.96 (br, 8H, $-CH_2$), 1.27 (br, 56H, $-CH_2$), 0.86 (br, 12 H, $-CH_3$). Anal. Calcd for PBDT-TBT: C, 69.15; H, 8.10; N, 2.52. Found: C, 68.51; H, 8.01; N, 2.51.

Poly{4,8-didodecyloxybenzo[1,2-*b*;3,4-*b*]dithiophene-*alt*-4,7-bis(4-hexylthiophen-2-yl)-5,6-bis(octyloxy)benzo-[*c*][1,2,5]thiadiazole} (PBDT-TBT-C6). The resulting copolymer PBDT-TBT-C6 was obtained as a dark powder with a yield of 81%. ^{1}H NMR (400 MHz, $CDCl_3$): δ (ppm) 8.52 (br, 2H, −Th), 7.60 (br, 2H, −Th), 4.37 (br, 4H, $-OCHH_2$), 4.22 (br, 4H, $-OCHH_2$), 3.04 (br, 4H, $-CH_2$), 1.96 (br, 12H, $-CH_2$), 1.27 (br, 68H, $-CH_2$), 0.86 (br, 18H, $-CH_3$). Anal. Calcd for PBDT-TBT-C6: C, 71.25; H, 8.91; N, 2.19. Found: C, 70.78; H, 8.57; N, 2.41.

Poly{4,8-didodecyloxybenzo[1,2-*b*;3,4-*b*]dithiophene-*alt*-5,6-bis(octyloxy)-4,7-bis(4-octylthiophen-2-yl)benzo[*c*]-[1,2,5]thiadiazole} (PBDT-TBT-C8). The resulting copolymer PBDT-TBT-C8 was obtained as a dark powder with a yield of 85%. ^{1}H NMR (400 MHz, $CDCl_3$): δ (ppm) 8.52 (br, 2H, −Th), 7.60 (br, 2H, −PM), 4.37 (br, 4H, $-OCHH_2$), 4.22 (br, 4H, $-OCHH_2$), 3.03 (br, 4H, $-CH_2$), 1.95 (br, 12H, $-CH_2$), 1.29 (br, 76 H, $-CH_2$), 0.87 (br, 18 H, $-CH_3$). Anal. Calcd for PBDT-TBT-C8: C, 71.85; H, 9.13; N, 2.10. Found: C, 71.66; H, 9.04; N, 2.22.

Poly{4,8-didodecyloxybenzo[1,2-*b*;3,4-*b*]dithiophene-*alt*-4,7-bis(4-decylthiophen-2-yl)-5,6-bis(octyloxy)benzo[*c*]-[1,2,5]thiadiazole} (PBDT-TBT-C10). The resulting copolymer PBDT-TBT-C10 was obtained as a dark powder with a yield of 81%. ^{1}H NMR (400 MHz, $CDCl_3$): δ (ppm) 8.52 (br, 2H, -Th), 7.59 (br, 2H, −Th), 4.37 (br, 4H, $-OCHH_2$), 4.22 (br, 4H, $-OCHH_2$), 3.03 (br, 4H, $-CH_2$), 1.97 (br, 12H, $-CH_2$), 1.29 (br, 84 H, $-CH_2$), 0.87 (br, 18 H, $-CH_3$). Anal. Calcd for PBDT-TBT-C10: C, 72.40; H, 9.34; N, 2.01. Found: C, 72.09; H, 9.52; N, 2.20.

Poly{4,8-didodecyloxybenzo[1,2-*b*;3,4-*b*]dithiophene-*alt*-4,7-bis(4-dodecylthiophen-2-yl)-5,6-bis(octyloxy)benzo-[*c*][1,2,5]thiadiazole} (PBDT-TBT-C12). The resulting copolymer PBDT-TBT-C12 was obtained as a dark powder with a yield of 76%. ^{1}H NMR (400 MHz, $CDCl_3$): δ (ppm) 8.52 (br, 2H, −Th), 7.60 (br, 2H, −Th), 4.37 (br, 4H, $-OCHH_2$), 4.22 (br, 4H, $-OCHH_2$), 3.03 (br, 4H, $-CH_2$), 1.97 (br, 12H, $-CH_2$), 1.29 (br, 92 H, $-CH_2$), 0.87 (br, 18 H, $-CH_3$). Anal. Calcd for PBDT-TBT-C12: C, 72.91; H, 9.53; N, 1.93. Found: C, 73.01; H, 9.76; N, 2.10.

Characterization. The elemental analysis was carried out with a Thermoquest CHNS-Ovelemental analyzer. The gel permeation chromatographic (GPC) analysis was carried out with a Waters 410 instrument with tetrahydrofuran as the eluent (flow rate: 1 mL/min, at 35 °C) and polystyrene as the standard. Thermogravimetric analysis were performed on a Perkin-Elmer Pyris 1 analyzer under nitrogen atmosphere (100 mL/min) at a heating rate of 10 °C/min. ^{1}H NMR and ^{13}C NMR spectra were measured using Inova nuclear magnetic resonance instruments. UV−visible absorption spectra were measured using a Shimadzu UV-3100 spectrophotometer. Electrochemical measurements of these derivatives were performed with a Bioanalytical Systems BAS 100 B/W electrochemical workstation. Atomic force microscopy (AFM) images of blend films were carried out using a Nanoscope IIIa Dimension 3100. The transmission electron microscopy (TEM) measurements were conducted on a HITACHI H-800 transmission electron microscope operated at 200 kV. Thin film X-ray diffraction (XRD) was recorded on a Bruker D8 Discover thin-film diffractometer with Cu KR radiation (λ = 1.54056 Å) operated at 40 keV and 40 mA.

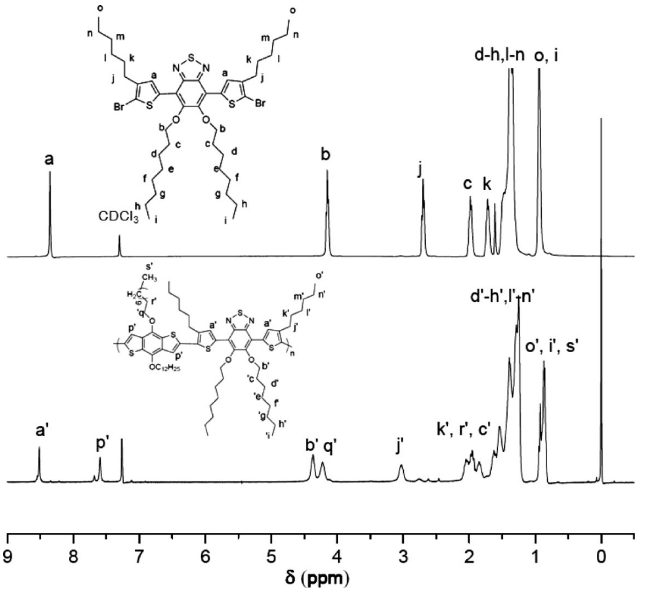

Figure 1. ^{1}H NMR spectrum and chemical structure of monomer BM-2 and copolymer PBDT-TBT-C6 in $CDCl_3$ solution.

Device Fabrication and Characterization. The active layer contained a blend of P3HT as electron donor and C_{60} derivatives as electron acceptor, which was prepared from varied weight ratios by solution (10 mg/mL of P3HT) in chlorobenzene. After spin coating the blend from solution at 600 rpm, the devices were completed by evaporating a 0.8 nm LiF layer protected by 100 nm of Al at a base pressure of 4×10^{-4} Pa. The effective photovoltaic area as defined by the geometrical overlap between the bottom ITO electrode and the top cathode was 12 mm^2. Current−voltage characteristics of the solar cells in the dark and under illumination of 100 mW/cm^2 white light from a Hg−Xe lamp filtered by a Newport 81094 Air Mass Filter, using a GWinstek SFG-1023 source meter. Monochromatic light from a Hg−Xe lamp (Newport 67005) in combination with monochromator (Oriel, Cornerstone 260) was modulated with a mechanical chopper. The response was recorded as the voltage over a 50 Ω resistance, using a lock-in amplifier (Newport 70104 Merlin). A calibrated Si cell was used as reference. All the measurements were performed under ambient atmosphere at room temperature. The optimized photovoltaic performance characteristics are given in Table 3.

RESULTS AND DISCUSSION

Synthesis and Characterization of Copolymers. We adopted the high coplanar and strong electron-donating ability BDT moiety as electron donor. The BDT moiety not only has a large planar conjugated structure and easily formed $\pi-\pi$ stacking, but also possesses low steric hindrance between adjacent units. This is because the 4,9-bis-alkoxy-BDT has no substituent on the 1, 3, 5, and 7 positions, which makes BDT an ideal conjugated unit for new photovoltaic material design.[30] The alkoxy-substituted 2,1,3-benzothiadiazoles was chosen as electron-accepting moiety, and connected with thiophene units containing different alkyl length to give compounds (TBT) from M-1 to M-5, which is then brominated with NBS to give monomer from BM-1 to BM-5. Finally, we used Pd(0)-catalyzed Stille coupling in toluene under heating to synthesize copolymers consisting of

Table 1. Polymerization Results for All the Copolymers

	M_n (kg/mol)[a]	M_w (kg/mol)[a]	PDI	T_d[b] (°C)
PBDT-TBT	62.9	95.7	1.52	312
PBDT-TBT-C6	43.5	113.6	2.62	327
PBDT-TBT-C8	23.8	50.4	2.12	331
PBDT-TBT-C10	28.3	93.1	2.78	321
PBDT-TBT-C12	32.3	85.8	2.65	329

[a] Calculated from GPC (eluent: $CHCl_3$; polystyrene standards). [b] Temperature at 5% weight loss by a heating rate of 10 °C/min under nitrogen.

TBT as electron-accepting moieties and BDT as an electron-donating moiety. The synthetic procedure for momoners and copolymers are shown in Scheme 1. The ^{1}H NMR spectrum of monomer BM-2 and copolymer PBDT-TBT-C6 in $CDCl_3$ solution are shown in Figure 1. All the hydrogens of monomer and copolymer have been given good adscriptions according to the corresponding chemical structure, which confirmed the success of copolymerization.

All the copolymers except PBDT-TBT exhibited good solubility in common organic solvents such as chloroform, tetrahydrofuran, and chlorobenzene. The worse solubility of PBDT-TBT may be caused by the high molecular weight and less flexible chains on the backbone. The molecular weights and polydispersities of the resulting polymers were determined by GPC analysis with number-average molecular weight (M_n) of 23.8−62.9 kg/mol and PDI (polydispersity index, M_w/M_n) of 1.5−2.8. The long alkoxy and alkyl chain on the monomers, which increases the solubility of intermediates during the polymerization, should be the main reason for the relative high polymerization degree. All the polymers exhibited good thermal stability with 5% weight-loss temperatures (T_d) higher than 312 °C under N_2, as revealed by thermogravimetric analysis (TGA) (see Figure S1, Supporting Information). The high thermal stability of the resulting polymers prevents the deformation of the polymer morphology and the degradation of the active layer in PVCs. Table 1 summarized the polymerization results including molecular weights, PDI and thermal stability of the copolymers.

Optical Properties. The normalized UV−vis absorption spectra of the copolymers in dilute chloroform solution (concentration 10^{-5} M) are shown in Figure 2a, and the main optical properties are listed in Table 2. The copolymer PBDT-TBT with alternating electron-donating BDT moiety and electron-accepting alkoxy-BT based TBT moiety showed three absorption peaks at 344, 412, and 549 nm in dilute solution UV−vis absorption spectra (Figure 2a), which can be assigned to the intrinsic absorption of the BDT moiety, the $\pi-\pi^*$ transition between BDT and TBT moiety of the conjugated polymer backbone, and ICT interaction between the BDT donor and TBT-based acceptor, respectively. Similarly, the absorption spectra of copolymers PBDT-TBT-C6, PBDT-TBT-C8, PBDT-TBT-C10, and PBDT-TBT-C12 with different alkyl chain length attaching to thiophene moiety showed almost the same, and it exhibited three absorption peaks around 342, 393, and 521 nm, respectively, which gives the similar assignments to the copolymer PBDT-TBT. It has to be noted that PBDT-TBT showed red-shifted absorption spectrum in chloroform solutions comparing other copolymers. Since there are less bulky groups in the PBDT-TBT copolymer, the coplanar property of BDT and TBT unit in the copolymer backbone is better than in other four copolymers, and results in stronger $\pi-\pi$ interactions between intermolecular

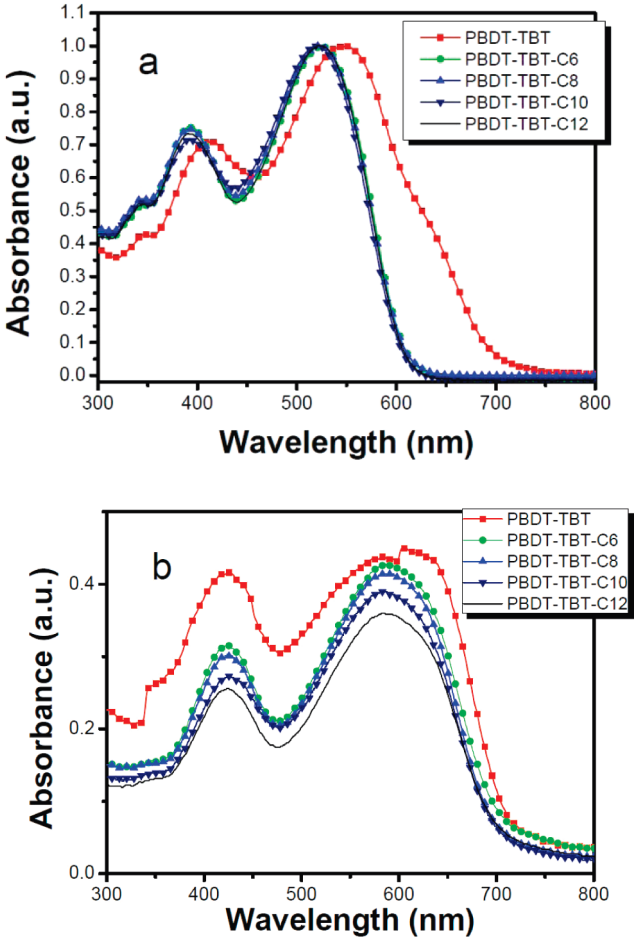

Figure 2. (a) Normalized absorption spectra of the copolymers in chloroform solutions with the concentration of 10^{-5} mol/L. (b) Films spin-coated from a 8−10 mg/mL chloroform solution with the thickness around 60 nm.

copolymers. This is proved by PBDT-TBT copolymer's increased crystallinity in solid state (as shown in Figure S2, Supporting Information) and decreased solubility in solvents. The blue-shifted absorption spectra of copolymers (PBDT-TBT-C6 to PBDT-TBT-C12) also indicated a more twisted backbone because of the long alkyl chain.[31] The twisted backbone can significantly reduce the conjugation length along the polymer backbone, resulting in a decrease in the ICT strength and thus electronic delocalization.[32] Meanwhile, the optical gap (absorption onset) and the absorption coefficients are not significantly affected by the length of alkyl chains. Moreover, the relatively high absorption coefficients (ε_{max}) could be calculated from the Beer law equation with the same dilute concentration of the copolymers in chloroform. The absorption spectra of the similar thickness copolymer films (around 60 nm) also showed similar absorption intensity, and the highest intensity reached 0.45, which assured the copolymers absorb enough photons.

Figure 2b shows the optical absorption spectra of thin films of the copolymers, and the optical properties are summarized in Table 2. The thin film absorption spectra are generally similar in shapes and trend to those in dilute solution. The maximum absorption peaks and absorption edge (λ_{edge}) in film were red-shifted by 57−67 nm and 17−99 nm, respectively, compared with those in solution, suggesting that intermolecular interactions

Table 2. Optical and Electrochemical Data of the Copolymers

	in solution[a]		in film[b]					
copolymer	λ_{max}^{abs} [nm] (ε_{max} [M^{-1} cm^{-1}])	λ_{edge} [nm]	λ_{max}^{abs} [nm]	λ_{edge} [nm]	E_{ox}^{onset} (V)/ HOMO(eV)	E_{red}^{onset} (V)/ HOMO(eV)	electrochem $E_{g,ec}$ (eV)	optical[c] $E_{g,ec}$ (eV)
PBDT-TBT	549 (40041)	691	606	708	0.52/−5.23	−1.16/−3.57	1.66	1.75
PBDT-TBT-C6	521 (49766)	609	588	704	0.55/−5.26	−1.16/−3.56	1.70	1.76
PBDT-TBT-C8	524 (45158)	611	589	700	0.58/−5.29	−1.16/−3.53	1.76	1.77
PBDT-TBT-C10	521 (49766)	609	584	700	0.54/−5.25	−1.15/−3.53	1.72	1.77
PBDT-TBT-C12	524 (42926)	608	588	707	0.52/−5.23	−1.12/−3.53	1.70	1.75

[a] 1×10^{-5} M in anhydrous chloroform. [b] Spin-coated from a 10 mg/mL chloroform solution. [c] The optical band gap ($E_{g,opt}$) was obtained from absorption edge.

were present in the solid state and were probably as strong as those of regioregular P3HT. Especially for the copolymers (PBDT-TBT-C6 to PBDT-TBT-C12) with different length alkyl chains attaching to thiophene moiety, the twisted backbone were extended and formed a higher coplanar backbone due to the $\pi-\pi$ stacking in film.[33] The optical band gaps $E_{g,opt}$ of the copolymers derived from the absorption edge of the thin film spectra are around 1.75 eV (Table 2), the low band gap can improve light harvesting and enhance the photocurrent of the PVCs.

Electrochemical Properties. The cyclic voltammetry (CV) diagrams of the copolymers were obtained by using $(TBA)PF_6$ as supporting electrolyte in acetonitrile solution with a platinum button working electrode, a platinum wire counter electrode, and a $Ag/AgNO_3$ reference electrode under the N_2 atmosphere. Ferrocene was used as the internal standard. The results of the electrochemical measurements are listed in Table 2. Because of the similar cyclic voltammetry curves of copolymers PBDT-TBT-C6, PBDT-TBT-C8, PBDT-TBT-C10, and PBDT-TBT-C12, Figure 3 shows only the cyclic volatammetry curves of copolymer PBDT-TBT and PBDT-TBT-C12. It can be seen from Figure 3 that there are irreversible p-doping/dedoping (oxidation/reduction) processes in the positive potential range for the copolymers. However, there are reversible n-doping/dedoping (reduction/reoxidation) processes in the negative potential range for the copolymers. Meanwhile, the onset oxidation (E_{ox}^{onset}) and reduction potential (E_{red}^{onset}) of all the copolymers are almost the same.

Since reduction potential of the D−A structure copolymer is mainly determined by the electron-accepting moiety,[34] all the copolymers, which have a same alkoxy-BT moieties with stronger electron-accepting ability, showed similar E_{red}^{onset}. Meanwhile, the copolymers also exhibited the nearly unchanged onset oxidation potential (E_{ox}^{onset}) (in the range of 0.52 to 0.58 V), which is caused by unchangeable electron-donating BDT and thiophene moieties. Therefore, it can be concluded that the alkyl with different length attached to the adjacent thiophene of BT-alkoxy moieties showed no effect on both the E_{red}^{onset} and E_{ox}^{onset}. The redox potential of Fc/Fc^+ which has an absolute energy level of −4.8 eV relative to the vacuum level for calibration is located at 0.08 V in 0.1 M $(TBA)PF_6$/acetonitrile solution.[35] So the evaluation of HOMO and LUMO levels, as well as the band gap ($E_{g,ec}$), could be done according to the following equations:

$$\text{HOMO (eV)} = -\text{e}(E_{ox}^{onset} + 4.72)\ \text{(eV)} \quad (1)$$

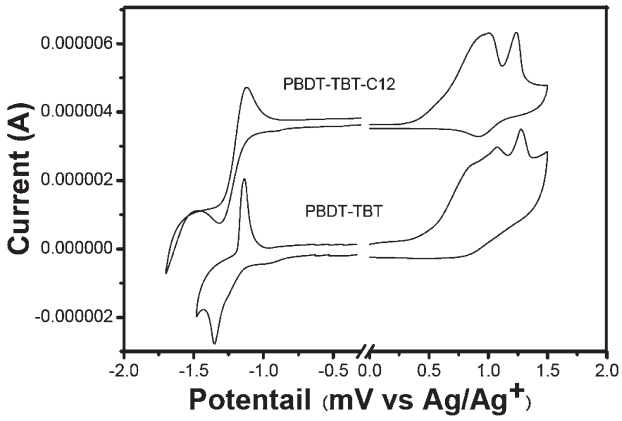

Figure 3. Cyclic voltammetry curves of copolymers films on platinum electrode in 0.1 mol/L n-Bu_4NPF_6 in CH_3CN solution, at a scan rate of 100 mV/s.

$$\text{LUMO (eV)} = -\text{e}(E_{red}^{onset} + 4.72)\ \text{(eV)} \quad (2)$$

$$E_{g,ec} = -(\text{HOMO} - \text{LUMO})\ \text{(eV)} \quad (3)$$

where E_{ox}^{onset} and E_{red}^{onset} are the measured potentials relative to Ag/Ag^+. The electrochemical properties as well as the energy level parameters of polymers are list in Table 2.

The estimated HOMO and LUMO energy levels of the copolymers are all around −5.25 and −3.53 eV, respectively. It indicated that the HOMO and LUMO energy levels of the copolymers are more dependent on the electron-donating and electron-accepting moiety, which can dominate the electronic delocalization intensity. In addition, the weak electron-donating alkyl chain attached to the adjacent thiophene of BT-alkoxy moieties did not affect the electron density distribution for both HOMO and LUMO energy level.

The energy levels of the donor polymers are very important for a high performance photovoltaic cell. First, the polymers should have good air stability with a HOMO energy level being below the air oxidation threshold (ca. −5.2 eV).[36] Second, the relatively low HOMO level of the polymers can allow a high open circuit voltage (V_{oc}) for the photovoltaic cell.[37] Third, the LUMO level of the donor has to be at least 0.3 eV higher than that of the acceptor (e.g., PCBM) to guarantee the formation of a downhill driving force for the energetically favorable electron transfer and

Table 3. Characteristic Current−Voltage Parameters From Device Testing at AM 1.5G White Light Conditions, Blend Films Roughness of AFM Measurement

	copolymer/PCBM (w/w ratio)	solvent	V_{oc} (V)	J_{sc}(mA/cm^2)	FF	PCE(%)	rms[c] (nm)
PBDT-TBT[a]	1:3	CB	0.68	3.48	0.47	1.11	2.33
PBDT-TBT-C6[a]	1:3	CB	0.74	4.50	0.44	1.92	0.83
PBDT-TBT-C8[a]	1:3	CB	0.70	7.19	0.52	2.88	1.73
PBDT-TBT-C10[a]	1:3	CB	0.72	3.95	0.37	1.04	4.86
PBDT-TBT-C12[a]	1:3	CB	0.71	2.19	0.33	0.51	5.13
PBDT-TBT-C8[b]	1:3	o-DCB	0.71	8.60	0.51	3.15	1.32

[a] The active layer based on the blend film of copolymers and $PC_{61}BM$. [b] The active layer based on the blend film of copolymers and $PC_{71}BM$. [c] Root mean-square (rms) roughness from AFM measurement.

to overcome the binding energy of the intrachain exciton.[38,39] The HOMO energy levels of the copolymers (around −5.25 eV) showed good air stability. Meanwhile, the LUMO energy levels difference between donor and acceptor is more than 0.3 eV, which guarantees the sufficient driving force for exciton dissociation. It is worth noting that the values of electrochemical band gap ($E_{g,ec}$) of copolymers are well consistent with that of optical band gap ($E_{g,opt}$).

Photovoltaic Properties. In order to investigate the photovoltaic properties of the copolymers, the BHJ photovoltaic cells, with a structure of ITO/PEDOT−PSS/Copolymers:PCBM/LiF/Al, were fabricated, where the copolymers were used as donors and $PC_{61}BM$ or $PC_{71}BM$ as acceptor. The active layers of the photovoltaic cells were fabricated from CB or *o*-DCB solutions of copolymers and $PC_{61}BM$ or $PC_{71}BM$ by spin-coating. Different conditions including the weight ratio between donor and acceptor and the thickness of the active layer were optimized. The optimized performances were achieved with the weight ratio of copolymers:$PC_{61}BM$ at 1:3 (w/w). The thickness of the active layer is 70−90 nm, which could be controlled by changing both the spin-coating rate and the concentration of the solution. Because of the high performance of PBDT-TBT-C8, we also fabricated the photovoltaic cell with the active layer (around 100 nm) prepared by spin-coating o-DCB solutions consisting of PBDT-TBT-C8 and $PC_{71}BM$ with the weight ratio of at 1:3 (w/w). All devices were characterized in the dark and under AM1.5 (100 mW/cm^2) white light with simultaneous recording of their current−voltage characteristics. The optimized photovoltaic performance characteristics of each PVCs are given in Table 3.

The obtained current−voltage curves are presented in Figure 4. The cell based on PBDT-TBT:$PC_{61}BM$ (1:3 w/w in CB solution) showed an open circuit voltage (V_{oc}) of 0.68 V, a short circuit current density (J_{sc}) of 3.48 mA/cm^2, a fill factor (FF) of 0.47, giving a PCE of 1.11%. Another two cells based on PBDT-TBT-C6:$PC_{61}BM$ and PBDT-TBT-C8:$PC_{61}BM$ showed V_{oc} of 0.74 and 0.70 V, significantly increasing J_{sc} to 4.50 and 7.16 mA/cm^2, FF to 0.44 and 0.52, and PCEs to 1.92% and 2.88%, respectively. The PCEs of the above two copolymer based devices were greatly improved by increasing the length of alkyl chains attached to thiophene moiety. However, with the length of alkyl chains continuously increased, the performances of the cells based on PBDT-TBT-C10:$PC_{61}BM$ and PBDT-TBT-C12:$PC_{61}BM$ were dropped, and showed J_{sc} of 3.95 and 2.19 mA/cm^2, V_{oc} of 0.72 and 0.71 V, PCEs of 1.04% and 0.51%, respectively.

It is generally considered that the V_{oc} is mainly determined by the difference between the HOMO energy level of the donor (copolymer) and LUMO energy level of the acceptor (PCBM).

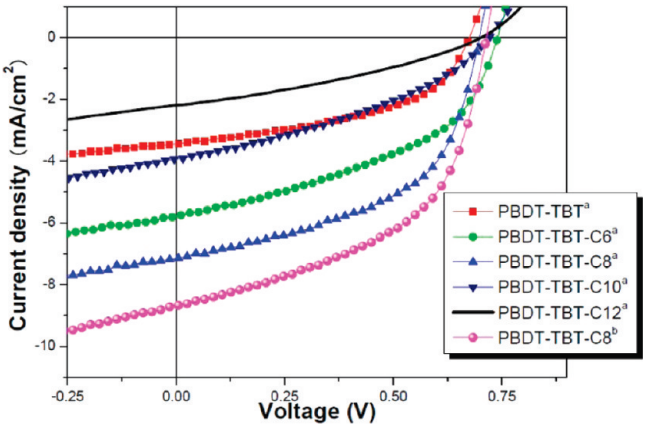

Figure 4. Current−voltage characteristics of optimized photovoltaic cells based on PBDT-TBT, PBDT-TBT-C6, PBDT-TBT-C8, PBDT-TBT-C10, and PBDT-TBT-C12 under illumination of AM 1.5, 100 mW/cm^2 white light. Key: (a) the active layer of copolymer and $PC_{61}BM$; (b) the active layer of copolymer and $PC_{71}BM$.

Because of the high electron-donating ability and excellent hole transporting properties of the two thiophene units bridged by benzene (BDT) moiety and the adjacent thiophene moieties of alkoxy-BT, the copolymers possessed relatively deeper HOMO energy level, which lead to the moderate V_{oc} (in the range of 0.68 to 0.74 V). Noticeably, with the increasing length of alkyl chains attached to thiophene moiety, the HOMO energy levels of the copolymers are almost the same, which may be caused by the weak electron-donating ability of alkyl chains. Meanwhile, the invariable HOMO energy levels also lead to the similar V_{oc}. Therefore, the well consistent tendency between HOMO energy level and V_{oc} of copolymers with varied length of alkyl chains further confirmed that the HOMO energy levels can effectively affect the V_{oc}. At the same time, the PBDT-TBT-C8:$PC_{61}BM$ based device also showed higher J_{sc} than the other four copolymer/$PC_{61}BM$ based devices, the reason for which is not as simple as that in the case of the V_{oc}. The J_{sc} of polymer/fullerene BHJ solar cells are influenced by their absorption spectrum, the carrier mobility and also the interpenetrating nanostructure formed by the blends of the copolymer and fullerene.

Film morphology of the active layer has been found to be one of the key elements in determining the PCE of polymer photovoltaic cell.[40,41] To gain better insight into what might control the short circuit current, and hence lead to the varied performances of PVCs, atomic force microscopy (AFM) and transmission

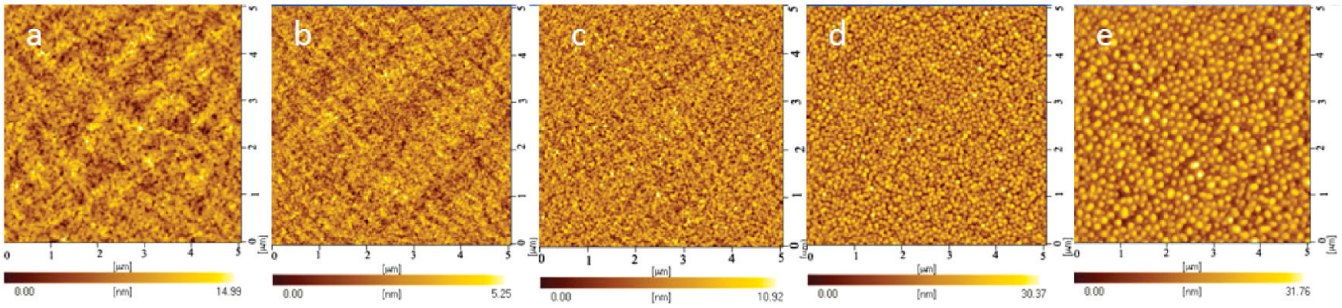

Figure 5. Topography image obtained by tapping-mode AFM showing the morphology of the blend films spin-coated from chlorobenzene for (a) PBDT-TBT/$PC_{61}BM$ (w/w, 1:4) (size 5 μm × 5 μm); (b) PBDT-TBT-C6/$PC_{61}BM$ (w/w, 1:3) (size 5 μm × 5 μm); (c) PBDT-TBT-C8/$PC_{61}BM$ (w/w, 1:3) (size 5 μm × 5 μm); (d) PBDT-TBT-C10/$PC_{61}BM$ (w/w, 1:3) (size 5 μm × 5 μm); and (e) PBDT-TBT-C12/$PC_{61}BM$ (w/w, 1:3) (size 5 μm × 5 μm).

electron microscopy (TEM) were used to examine the topography of the active layer. Here, the AFM height topography image were mainly used to investigate the surface morphology of the active layer, which can obtain the roughness and aggregation of the blend film, hence it reflect the solubility of the copolymers and the miscibility between the copolymer and $PC_{61}BM$. Figure 5a shows the AFM height images of PBDT-TBT:$PC_{61}BM$ blend film with the optimized weight ratio (1:3 w/w). As is clearly evidenced by AFM, the PBDT-TBT:$PC_{61}BM$ blend film showed a relative higher coarse surface with the root-mean-square (rms) of 2.33 nm (Figure 5a and Table 3), and larger PCBM aggregation compared with that obtained at a blend film of PBDT-TBT-C6:$PC_{61}BM$ (rms = 0.83 nm). The rougher surfaces of PBDT-TBT:$PC_{61}BM$ blend film presumably arose from poor solubility of the copolymer PBDT-TBT (no alkyl chains attached to thiophene moiety), which leads to aggregation of PCBM that might limit the degree of charge dissociation and reduce the photocurrent. In the case of copolymer PBDT-TBT-C6 (Figure 5b), where the alkyl chains (six carbons) attached to thiophene moiety, the smooth surface of the blend film PBDT-TBT-C6:$PC_{61}BM$ indicates the good solubility of the PBDT-TBT-C6 and better miscibility between PBDT-TBT-C6 and $PC_{61}BM$, which leads to the improved J_{sc} of PBDT-TBT-C6:$PC_{61}BM$ cell (4.5 mA/cm^2). This result implies that there is still room for improvement in terms of the charge separation interface in copolymer/$PC_{61}BM$. With the continuous increase length of alkyl chains (eight carbon) attached to thiophene moiety, the morphology of PBDT-TBT-C8:$PC_{61}BM$ blend film (Figure 5c) shows no obvious aggregation of PCBM and the rms increases to 1.73 nm, which leads to the great increase of J_{sc} (7.19 mA/cm^2). Interestingly, when the length of alkyl chains continually increased to ten and 12 carbons, the grain-aggregation in the blend film PBDT-TBT-C10:$PC_{61}BM$ and PBDT-TBT-C12:$PC_{61}BM$ appeared again (as shown in Figure 5d,e), and the aggregated PCBM was almost homogeneously dispersed in the copolymers matrix (rms is 4.86 and 5.13 nm, respectively). This resulted in a large-scale phase separation between copolymers and $PC_{61}BM$, and hence decreased J_{sc} to 3.95 and 2.19 mA/cm^2 based on the devices of PBDT-TBT-C10:$PC_{61}BM$ and PBDT-TBT-C12:$PC_{61}BM$, respectively. The degenerated device performances may be caused by the decreased diffusional escape probability for the mobile charge carriers and increased recombination. It is important to note that even though the PBDT-TBT-C8:$PC_{61}BM$ blend film shows a relatively rough morphology in the AFM height image, among all the material combinations, the solar cells of PBDT-TBT-C8:$PC_{61}BM$ gave the highest J_{sc}, suggesting the appropriate coarse phase separation between the copolymers and $PC_{61}BM$ in these cells. Meanwhile, the FF show the decreased values from 0.33 to 0.52 for the increasing aggregation of $PC_{61}BM$. From these results, it is clear that the dramatic varied J_{sc} and FF observed in the copolymer:PCBM photovoltaic devices is mostly due to the morphology problem coming from poor miscibility and different self-assembly property between the copolymers and $PC_{61}BM$.

The purported ideal morphology is comprised of an nanoscale interpenetrating network between donor and acceptor, which enables a large interface area for exciton dissociation and continuous percolating paths for hole and electron transport to the corresponding electrodes.[42] In order to further investigate the relation between the blend film morphology and J_{sc}, the copolymers:PCBM blend films were observed by TEM (Figure 6), which can directly determine the composition and more real morphology of the blend film comparing with the AFM morphology. The polymer networks and porous regions are imaged in the TEM as darker (PCBM) and lighter (copolymer) colored, respectively.[43] From the TEM images of the PBDT-TBT:$PC_{61}BM$ (1:3 w/w) blend films (Figure 6a), which have no alkyl chains attached to thiophene moiety, we can observe substantial pea-like PCBM aggregation with obvious phase separation. In the case of PBDT-TBT-C6:$PC_{61}BM$ blend film (Figure 6b), the alkyl chain with six carbon was attached to thiophene moiety, the PCBM aggregation disappeared completely and the blend film exhibited very smooth surface morphology and uniform mixing, which can be further confirmed by the low rms value of its corresponding AFM image. In contrast, the TEM images of PBDT-TBT-C8:$PC_{61}BM$ blend film showed nanoscale interpenetrating network with a finer porous and nanoscale phase separation structure (Figure 6c), which can facilitate better percolation of the carriers and hence lead to the highest J_{sc} of 7.19 mA/cm^2. Accordingly, the proper nanoscale phase separation with no obvious aggregation between electron donor and acceptor molecules allows for large areas of interfaces for better photogenerated charges and desirable J_{sc}. Meanwhile, the sufficient carrier separation on interface can also decrease the possibility of recombination of holes and electrons in the network with high interfacial areas, which lead to a reduced series resistance. This might be the reason why the PBDT-TBT-C8:$PC_{61}BM$ based devices possess higher FF values (0.52).[44] Noticeably, with the increasing length of alkyl chains, the TEM images of the PBDT-TBT-C10:$PC_{61}BM$ and PBDT-TBT-C12:$PC_{61}BM$ (Figure 6d,e) showed a larger size

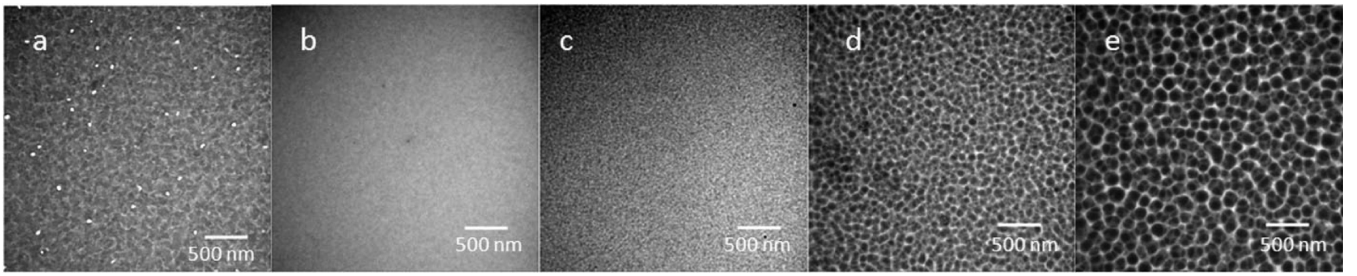

Figure 6. TEM image obtained by the blend films spin-coated from chlorobenzene for (a) PBDT-TBT/$PC_{61}BM$ (w/w, 1:3); (b) PBDT-TBT-C6/$PC_{61}BM$ (w/w, 1:3); (c) PBDT-TBT-C8/$PC_{61}BM$ (w/w, 1:3); (d) PBDT-TBT-C10/$PC_{61}BM$ (w/w, 1:3); and (e) PBDT-TBT-C12/$PC_{61}BM$ (w/w, 1:3).

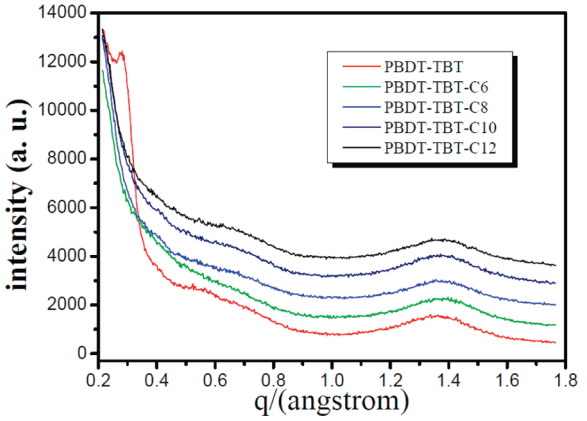

Figure 7. XRD patterns of blend films spin-coated from chlorobenzene for copolymers (PBDT-TBT, PBDT-TBT-C6, PBDT-TBT-C8, PBDT-TBT-C10, and PBDT-TBT-C12)/$PC_{61}BM$ (w/w, 1:3).

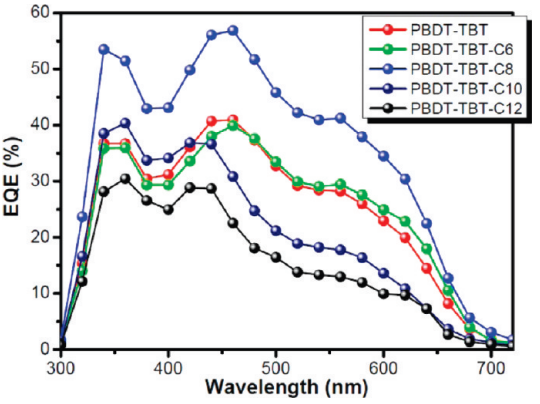

Figure 8. External quantum efficiencies (EQE) spectra of devices based on copolymers:$PC_{61}BM$.

grain-like aggregation. Because of the limited diffusion length of excitons (10 nm), which is much smaller than the size grain-like aggregation (50−200 nm) seen in the blend film images of PBDT-TBT-C10:$PC_{61}BM$ and PBDT-TBT-C12:$PC_{61}BM$, photogenerated excitons will mainly recombine before reaching the interfaces of the donor and acceptor, resulting in reduced charge carrier generation and a concomitant loss of photocurrent (reduce to 3.95 mA/cm^2 and 2.19 mA/cm^2). The nonoptimized morphology can reduce hole or electron drift length (or both of holes and electrons). The space charge accumulation caused by sluggish charge carriers subsequently induces a nonuniform electric field, which gives rise to a decreased photocurrent with strong electric field dependence, resulting in low FF (0.37 and 0.33).[45] These results showed that solar cell properties strongly depend on the solid-state structures, and also fully demonstrated that the morphology of the blend film can be well controlled by molecular engineering of the copolymers. The different miscibility and self-assembly structure between copolymer and $PC_{61}BM$ can significantly influence transport properties, J_{sc} and *FF* of the device to a large extent. Control of the blend film morphology between copolymer and $PC_{61}BM$ and the formation of interpenetrating network structure domains may improve charge transport, depress leakage current, and, in turn, increase J_{sc}, FF, and even V_{oc}.

Besides the miscibility with $PC_{61}BM$, the varied crystallinity and molecular packing of the copolymers in the blend films may also influence the device efficiency. As shown in Figure 7, XRD studies revealed the crystallinity and π-stacking of the copolymers in blend film. Only the PBDT-TBT/$PC_{61}BM$ film showed a peak at q = 0.28 Å, which indicates that the copolymer PBDT-TBT without alkyl chain substitution on the thiophene moiety crystallized in the blend film.[25] The crystallization of copolymer can increase the ordering in blend film which can facilitate the electronic communication across the interface and enhance hole extraction and block undesired electron leakage. Therefore, device based on the PBDT-TBT/$PC_{61}BM$ lead to the relative high FF (0.47). All the blend films showed the same $\pi-\pi$ stacking peaks at around q = 1.38 Å, which indicates that the varied alkyl chain substitution attached to the thiophene unit may not affect the $\pi-\pi$ stacking (d spacing with 4.55 Å) interaction significantly in this polymer series, but presumably affects PCBM interactions with the varied alkyl chain of copolymers, which have been confirmed in the morphology characterization. The unchanged $\pi-\pi$ stacking d spacing values (4.55 Å) of copolymers with varied alkyl chain are well consistent with the Chen's report of the $\pi-\pi$ stacking spacing in films.[26]

The external quantum efficiencies (EQE) of PVCs based on all the copolymers blended with $PC_{61}BM$ under monochromatic illumination are shown in Figure 8. The shape of the EQE curve of the devices based on copolymer:PCBM are very similar to their absorption spectrum, indicating that most of the absorptive photons of the copolymer contributed to the photovoltaic conversion. The spectral responses of the five copolymer:$PC_{61}BM$ based devices reveal significant contributions of the EQE at wavelengths between 300 and 700 nm, with the maximum EQE

in the range of 57% to 29% at around 460 nm. Meanwhile, the J_{sc} calculated from the EQE are well consistent with the measured J_{sc} in trend. It is worth noting that the maximum spectral responses wavelength of the blend film morphologies with larger phase separation (PBDT-TBT-C10 and PBDT-TBT-C12) are generally blue shift about 20 nm comparing with that obtained from the smooth or uniform blend film (PBDT-TBT, PBDT-TBT-C6, and PBDT-TBT-C10), which may be caused by the reduced charge carrier generation and a concomitant loss of photocurrent. Because of the high performance of the device based on the PBDT-TBT-C8/$PC_{61}BM$ and the better absorption spectrum of $PC_{71}BM$ as an acceptor, the device based on the PBDT-TBT-C8:$PC_{71}BM$ in o-DCB solution was prepared. The device shows a V_{oc} of 0.71 V, a J_{sc} of 8.60 mA/cm^2, a FF of 0.51, and a PCE of 3.15%.

CONCLUSIONS

We have designed and synthesized a series of high coplanar D−A copolymers with varied alkyl chain attached to thiophene moiety through Stille coupling polymerization. We observed that varied alkyl chain with weak electron donating ability attached to thiophene moiety exhibited no obvious effect on the optical, electrochemical property, and all the copolymers possess narrow optical band gaps around 1.75 eV. Although the copolymers showed the similar optical and electrochemical properties, mutual miscibility between the donor copolymer and the acceptor fullerene derivative can dramatically affect the solar cell power output. In this work, varied alkyl chain substitution provided the driving force for the phase separation of the copolymer/$PC_{61}BM$ blend film, and thus controlled the blend film phase separation. TEM observations revealed the morphologies of the blend film of the copolymer and $PC_{61}BM$ changed from a pea-like aggregation to an interpenetrating network to a grain-like structure. The PVCs based on the copolymers were fabricated with a structure of ITO/PEDOT:PSS/polymers:$PC_{61}BM$/Al under the illumination of AM 1.5G, 100 mW/cm^2. The photovoltaic performances of these copolymers varied significantly, and the best performance of PVCs was obtained by using PBDT-TBT-C8:$PC_{61}BM$ as the active layer with a PCE of 2.88%, an open-circuit voltage (V_{oc}) of 0.70 V, a short-circuit current (J_{sc}) of 7.19 mA/cm^2, a fill factor (*FF*) of 0.52. The corresponding active layer exhibited interpenetrating network morphology, which enhanced the device properties through more efficient charge transport. The EQEs of all the devices can also well confirm the photovoltaic performances. PVC with the highest power conversion efficiency of 3.15% was observed when the PBDT-TBT-C8 was blended with $PC_{71}BM$ acceptor.

ASSOCIATED CONTENT

Supporting Information. TGA curves and X-ray diffraction (XRD) patterns of the copolymers. This material is available free of charge via the Internet at http://pubs.acs.org.

AUTHOR INFORMATION

Corresponding Author

*E-mail: tuyingfeng@suda.edu.cn. Telephone: +86512 65882130. Fax: +86512 65882130.

ACKNOWLEDGMENT

The financial support from the National Nature Science Foundation of China (No. 21074079), Key Project in Science & Technology Innovation Cultivation Program of Soochow University, a Project Funded by the Priority Academic Program Development of Jiangsu Higher Education Institutions, and National "973" Project (2011CB606004) is gratefully acknowledged.

REFERENCES

(1) Tang, C. W. *Appl. Phys. Lett.* **1986**, *48*, 183–185.
(2) Yu, G.; Gao, J.; Hummelen, J. C.; Wudl, F.; Heeger, A. J. *Science* **1995**, *270*, 1789–1791.
(3) Gunes, S.; Neugebauer, H.; Sariciftci, N. S. *Chem. Rev.* **2007**, *107*, 1324–1338.
(4) Sacriciftci, N. S.; Smilowitz, L.; Heeger, A. J.; Wudl, F. *Science* **1992**, *258*, 1474–1476.
(5) Ma, W. L.; Gopinathan, A.; Heeger, A. J. *Adv. Mater.* **2007**, *19*, 3656–3659.
(6) Nguyen, L. H.; Hoppe, H.; Erb, T.; Günes, S.; Gobsch, G.; Sariciftci, N. S. *Adv. Funct. Mater.* **2007**, *17*, 1071–1078.
(7) Kim, Y.; Choulis, S. A.; Nelson, J.; Bradley, D. D. C. *Appl. Phys. Lett.* **2005**, *86*, 063502.
(8) He, F.; Wang, W.; Chen, W.; Xu, T.; Darling, S. B.; Strzalka, J.; Liu, Y.; Yu, L. P. *J. Am. Chem. Soc.* **2011**, *133*, 3284–3287.
(9) Son, H. J.; Wang, W.; Xu, T.; Liang, Y. Y.; Wu, Y.; Li, G.; Yu, L. P. *J. Am. Chem. Soc.* **2011**, *133*, 1885–1894.
(10) Qin, R. P.; Li, W. W.; Li, C. H.; Du, C.; Veit, C.; Schleiermacher, H. F.; Andersson, F.; Bo, Z. S.; Liu, Z. P.; Inganäs, O.; Wuerfel, U.; Zhang, F. L. *J. Am. Chem. Soc.* **2009**, *131*, 14612–14613.
(11) Chen, H. Y.; Hou, J. H.; Zhang, S. Q.; Liang, Y. Y.; Yang, G. W.; Yang, Y.; Yu, L. P.; Wu, Y.; Li, G. *Nat. Photonics* **2009**, *3*, 649–653.
(12) Chen, C. P.; Chan, S. H.; Chao, T. C.; Ting, C.; Ko, B. T. *J. Am. Chem. Soc.* **2008**, *130*, 12828–12833.
(13) Qin, R. P.; Li, W. W.; Li, C. H.; Du, C.; Veit, C.; Schleiermacher, H. F.; Andersson, F.; Bo, Z. S.; Liu, Z. P.; Ingan€as, O.; Wuerfel, U.; Zhang, F. L. *J. Am. Chem. Soc.* **2009**, *131*, 14612–14613.
(14) Blouin, N.; Michaud, A.; Gendron, D.; Wakim, S.; Blair, E.; Plesu, R. N.; Bellette, M.; Durocher, G.; Tao, Y.; Leclerc, M. *J. Am. Chem. Soc.* **2008**, *130*, 732–742.
(15) Kroon, R.; Lenes, M.; Hummelen, J. C.; Blom, P. W. M.; de Boer, B. *Polym. Rev.* **2008**, *48*, 531–582.
(16) Li, Y. W.; Xue, L. L.; Li, H.; Li, Z. F.; Xu, B.; Wen, S. P.; Tian, W. J. *Macromolecules* **2009**, *42*, 4491–4499.
(17) Bijleveld, J. C.; Gevaerts, V. S.; Nuzzo, D. D.; Turbiez, M.; Mathijssen, S. G. J.; Leeuw, D. M. D.; Wienk, M. M.; Jassen, R. A. J. *Adv. Mater.* **2010**, *22*, E242–E246.
(18) Zhang, L. J.; He, C.; Chen, J. W.; Yuan, P.; Huang, L.; Zhang, C.; Cai, W. Z.; Liu, Z. T.; Caok, Y. *Macromolecules* **2010**, *43*, 9771–9778.
(19) Cheng, Y. J.; Hsieh, C. H.; He, Y. J.; Hsu, C. S.; Li, Y. F. *J. Am. Chem. Soc.* **2010**, *132*, 17381–17383.
(20) Cheng, Y. J.; Yang, S. H.; Hsu, C. S. *Chem. Rev.* **2009**, *109*, 5868–5923.
(21) Ma, W. L.; Yang, C. Y.; Gong, X.; Lee, K.; Heeger, A. J. *Adv. Funct. Mater.* **2005**, *15*, 1617–1622.
(22) Zhang, F. L.; Jespersen, K. G.; Björström, C.; Svensson, M.; Andersson, M. R.; Sundström, V.; Magnusson, K.; Moons, E.; Yartsev, A.; Inganäs, O. *Adv. Funct. Mater.* **2006**, *16*, 667–674.
(23) Peet, J.; Kim, J. Y.; Coates, N. E.; Ma, W. L.; Moses, D.; Heeger, A. J.; Bazan, G. C. *Nat. Mater.* **2007**, *6*, 497–500.
(24) Li, Y. W.; Xu, B.; Li, H.; Cheng, W. D.; Xue, L. L.; Chen, F. P.; Lu, H. G.; Tian, W. J. *J. Phys. Chem. C* **2011**, *115*, 2386–2397.
(25) Piliego, C.; Holcombe, T. W.; Douglas, J. D.; Woo, C. H.; Beaujuge, P. M.; Fréchet, J. M. *J. Am. Chem. Soc.* **2010**, *132*, 7595–7597.
(26) Szarko, J. M.; Guo, J.; Liang, Y.; Lee, B.; Rolczynski, B. S.; Strzalka, J.; Xu, T.; Loser, S.; Marks, T. J.; Yu, L.; Chen, L. X. *Adv. Mater.* **2010**, *22*, 5468–5472.
(27) Wu, P. Z.; Ren, G.; Jenekhe, S. A. *Macromolecules* **2010**, *43*, 3306–3313.

(28) Liang, Y. Y.; Xu, Z.; Xia, J. B.; Tsai, S. T.; Wu, Y.; Li, G.; Ray, C.; Yu, L. P. *Adv. Mater.* **2010**, *22*, E135–E138.
(29) Liang, Y. Y.; Feng, D. Q.; Wu, Y.; Tsai, S. T.; Li, G.; Ray, C.; Yu, L. P. *J. Am. Chem. Soc.* **2009**, *131*, 7792–7799.
(30) Hou, J.; Park, M. H.; Zhang, S.; Yao, Y.; Chen, L. M.; Li, J. H.; Yang, Y. *Macromolecules* **2008**, *41*, 6012–6018.
(31) Helgesen, M.; Gevorgyan, S. A.; Krebs, F. C.; Jansse, R. A. J. *Chem. Mater.* **2009**, *21*, 4669–4675.
(32) Wu, P. T.; Kim, F. S.; Champion, R. D.; Jenekhe, S. A. *Macromolecules* **2008**, *41*, 7021–7028.
(33) Liu, J. Y.; Zhang, R.; Sauvé, G.; Kowalewski, T.; McCullough, R. D. *J. Am. Chem. Soc.* **2008**, *130*, 13167–13176.
(34) Huo, L. J.; Hou, J. H.; Chen, H. Y.; Zhang, S. Q.; Jiang, Y.; Chen, T. L.; Yang, Y. *Macromolecules* **2009**, *42*, 6564–6571.
(35) Pommerehne, J.; Vestweber, H.; Guss, W.; Mahrt, R. F.; Bassler, H.; Porsch, M.; Daub, J. *Adv. Mater.* **1995**, *7*, 551–554.
(36) Leeuw, D. M. D.; Simenon, M. M. J.; Brown, A. R.; Einerhand, R. E. F. *Synth. Met.* **1997**, *87*, 53–59.
(37) Leclerc, N.; Michaud, A.; Sirois, K.; Morin, J.-F.; Leclerc, M. *Adv. Mater.* **2006**, *16*, 1694–1704.
(38) Koster, L. J. A.; Mihailetchi, V. D.; Blom, P. W. M. *Appl. Phys. Lett.* **2006**, *88*, 093511.
(39) Brabec, C. J.; Winder, C.; Sariciftic, N. S.; Hummelen, J. C.; Dhanabalan, A.; van Hal, P. A.; Janssen, R. A. J. *Adv. Funct. Mater.* **2002**, *12*, 709–712.
(40) Peet, J.; Kim, J. Y.; Coates, N. E.; Ma, W. L.; Moses, D.; Heeger, A. J.; Bazan, G. C. *Nat. Mater.* **2007**, *6*, 497–500.
(41) Li, G.; Shrotriya, V.; Huang, J.; Yao, Y.; Moriarty, T.; Emery, K.; Yang, Y. *Nat. Mater.* **2005**, *4*, 864–868.
(42) Li, Y. W.; Guo, Q.; Li, Z. F.; Pei, J. N.; Tian, W. J. *Energy Environ. Sci.* **2010**, *3*, 1427–1436.
(43) Babel, A.; Jenekhe, S. A. *J. Phys. Chem. B* **2003**, *107*, 1749–1754.
(44) Dennler, G.; Scharber, M. C.; Brabec, C. J. *Adv. Mater.* **2009**, *21*, 1323–1338.
(45) Mihailetchi, V. D.; Wildeman, J.; Blom, P. W. M. *Phys. Rev. Lett.* **2005**, *94*, 126602.